ELSEVIER

Spectrochimica Acta Part B 61 (2006) 340–350

SPECTROCHIMICA ACTA PART B

www.elsevier.com/locate/sab

Spectroscopic and shadowgraphic analysis of laser induced plasmas in the orthogonal double pulse pre-ablation configuration

G. Cristoforetti *, S. Legnaioli, L. Pardini, V. Palleschi, A. Salvetti, E. Tognoni

Applied Laser Spectroscopy Laboratory, Institute for Chemical–Physical Processes Research Area of National Research Council, Via G. Moruzzi, 1-56124 Pisa, Italy

Received 12 December 2005; accepted 4 March 2006

Abstract

This work focuses on the study of the plumes obtained in the double pulse orthogonal Laser Induced Breakdown Spectroscopy (LIBS) in the pre-ablation configuration using both spectroscopic and shadowgraphic approaches. Single and double pulse LIBS experiments were carried out on a brass sample in air. Both the distance of the air plasma from the target surface and the interpulse delay were varied (respectively in the range 0.1–4.2 mm and up to 50 μs) revealing a significant variation of the plasma emission and of the plume-shock wave dynamical expansion in different cases. The intensity of both atomic and ionized zinc lines was measured in all the cases, allowing the calculation of the spatially averaged temperature and electron density and an estimation of the ablated mass. The line intensities and the thermodynamic parameters obtained by the spectroscopic measurements were discussed bearing in mind the dynamical expansion characteristics obtained from the shadowgraphic approach. All the data seem to be consistent with the model previously proposed for the double pulse collinear configuration where the line enhancement is mainly attributed to the ambient gas rarefaction produced by the first laser pulse, which causes a less effective shielding of the second laser pulse.

Keywords: Laser induced breakdown spectroscopy; Double pulse; Shadowgraphy; Shock wave

1. Introduction

Laser Induced Breakdown Spectroscopy (LIBS) is a well known analytical technique for determining the chemical elementary composition of solid, liquid, gaseous and aerosols samples. The simplicity of its basic idea, i.e. the spectroscopic analysis of radiation emitted by a micro-plasma induced on the sample by a laser pulse, makes such technique very attractive for a large variety of applications [1], including in situ analyses. On the other hand, the limits of detection of LIBS, which are typically of the order of ppm or tens of ppm for most of the elements, are poorer with respect to other more traditional analytical techniques (e.g. ICP-MS and ICP-OES). The Double Pulse (DP)-LIBS configuration, which makes use of two laser pulses separated by a suitable temporal delay instead of a single pulse (SP) for inducing the plasma, has been extensively studied in recent years since it is reported to give a substantial enhancement of the signal to noise ratio with respect to single pulse LIBS configuration with a corresponding improvement of the limits of detections.

Several DP configurations have been studied, differing on the geometrical arrangement, the wavelength and the timing of the two laser beams. While most research efforts have been focused on the collinear configuration, where both beams are aligned normally to the target and are focused on its surface [2–8], the orthogonal configuration has also been tested. Here, the first pulse (pre-ablation scheme) [9–13] or the second one (re-heating scheme) [12,14] is directed parallel to the target surface and focused in the air in front of it, while the other is perpendicular and ablates the target.

While the physical mechanism occurring in the orthogonal reheating scheme involves the absorption of the second beam by the pre-existing plasma, the reason of the signal enhancement in the other experimental schemes — which can reach two orders

* Corresponding author. Tel.: +39 050 3152222; fax: +39 050 3152230.
E-mail address: gabriele@ipcf.cnr.it (G. Cristoforetti).

0584-8547/$ - see front matter © 2006 Elsevier B.V. All rights reserved.
doi:10.1016/j.sab.2006.03.004

of magnitude depending on the experimental conditions and on the sample matrix — is not univocally determined.

In spite of the obvious differences between the collinear and the pre-ablation experimental apparatus, the experimental results show an interesting number of similarities. In both cases, the signal enhancement cannot be attributed to a simple re-heating of the existing plasma by the second laser pulse, since the slight rise of plasma temperature usually observed cannot justify the enhancement measured [3,9]. On the other hand, in several works using these configurations the high emission signal is associated to a relevant increase of mass removal from the target, to a faster dynamic evolution of the plume and to a larger volume of plasma emission with respect to the SP case [4,5,9].

Our previous studies on DP LIBS in collinear configuration, all devoted to identify the main reasons of the signal enhancement, were focused on a comparison of time- and space-resolved emission of the plumes in SP and DP configurations [15], on the effect of different ambient gas pressures and different interpulse delays observed with spectroscopic [16] and imaging techniques [17], and finally on the effect of changing the laser pulses energies on the DP signal and on the craters produced on the target [18]. In the light of the results obtained, a phenomenological model was proposed where, as also suggested by Pershin [19], the high DP signal is due to a very efficient ablation process, caused by the second pulse impinging on the target surface in an ambient gas condition substantially different from the unperturbed state. In fact, the blast wave produced by the first laser pulse, according to the strong point explosion theory formulated by Sedov [20], expands in the air leaving behind a rarefied atmosphere, where a better coupling between the second laser pulse and the target is obtained.

In this work we investigated the DP LIBS in the orthogonal pre-ablation scheme, originally introduced in Refs. [9–11] wherein the effect of pulse delay on the signal, on the mass removal from the target and on the temperature of the plasma was extensively studied. According to the interpretation reported [21], the observed signal enhancement is probably due to the concurrence of different effects, i.e. pre-ionization of air causing a better laser-plasma coupling (via a more efficient inverse Bremsstrahlung process), different pressure-density conditions of ambient gas during the second laser ablation and pre-heating of the target, which play a different role at different inter-pulse delays. The hypothesis of ambient pressure change to justify the signal improvement was also suggested by Gautier et al. [12] and Lindner et al. [13], who reported a dependence of signal enhancement on the excitation energy levels and a better atomization in the pre-ablation scheme, respectively.

The basic idea underlying this work is that the model proposed in collinear DP LIBS should work well also in the orthogonal pre-ablation scheme since the blast wave produced in air expands, interacts with target, is reflected and then leaves in front of the target a rarefied gas atmosphere. Moreover, a substantially different hydrodynamic evolution of the blast wave and of the ambient gas thermodynamic parameters is expected with changing the distance between the parallel laser beam and the target. The aim of the paper is to study the emission behavior observed in the pre-ablation scheme at different values of such parameter. A direct imaging of the expansion of the shock waves and plumes produced by the two laser pulses was also obtained by shadowgraphic analysis.

2. Experimental

In order to analyze the processes of laser ablation and plasma formation obtained in the double pulse orthogonal pre-ablation LIBS configuration, two different experimental approaches were used. At first, the spectrally-resolved emission from the plasma was obtained; then the results were compared with the temporally resolved images of the plume acquired using the shadowgraphic technique.

The experimental setup combining both the spectroscopic and shadowgraphic techniques is sketched in Fig. 1.

The laser sources were two Nd:YAG lasers (Quanta System Handy 100 and Lumonics HY100), each one emitting a laser pulse in 8 ns FWHM at the wavelength of 1.06 μm. Bearing in mind that the amount of energy delivered by the second laser pulse affects the signal enhancement in the DP configuration much more than the energy of the first pulse [12,18], the energies of the first and second laser pulses were adjusted to 140 and 240 mJ, respectively.

The two laser beams were aligned in an orthogonal configuration, so that the first one (Quanta System Handy 100) was directed parallel to the surface of a target — a ~ 60% Cu, ~ 40% Zn brass alloy — and then focused in front of it by means of a 30-cm focal length lens (the waist obtained was ~ 50 μm), while the second one was directed perpendicularly and focused on the target surface by using a 10 cm focal length lens. The focus of this second lens was set a couple of millimeters under the target surface in order to improve the reproducibility of the micro-plasma [22].

The distance between the focus of the parallel beam lens and the target surface (hereafter named d) was varied in the range 0.1–4.2 mm by slightly shifting the lateral position of the lens; the spectroscopic analysis of signal obtained by using only the pre-ablation laser in air could not evidence a detectable emission from target species even in the case of $d = 0.1$ mm, indicating that the mass removal from the target is negligible for all the values of the parameter d.

The delay between the laser pulses was changed by means of a delay generator and monitored during the experiment by sending a small fraction of the laser beams to a fast photodiode coupled to a digital oscilloscope. The measured temporal jitter of each laser pulse with respect to the other was within ±20 ns.

For the spectroscopic measurements, the space-integrated LIBS signal was collected through an optical quartz fiber (diameter = 0.6 mm, N.A. = 0.22), placed at 45° with respect to the target surface at a 3-cm distance from the plume. The optical signal was then sent to an Echelle spectrometer ($\lambda/\Delta\lambda = 7500$) coupled with an intensified CCD camera, which provided for each acquisition a full spectrum in the range 200–900 nm.

A delay time of acquisition of 500 ns was chosen together with a measuring gate of 500 ns. The integration window was chosen in order to allow the decay of continuum, due to *Bremsstrahlung* radiation and free-bound electronic recombination, and to assure an adequate signal to noise ratio for both atomic and ionized lines from matrix elements.

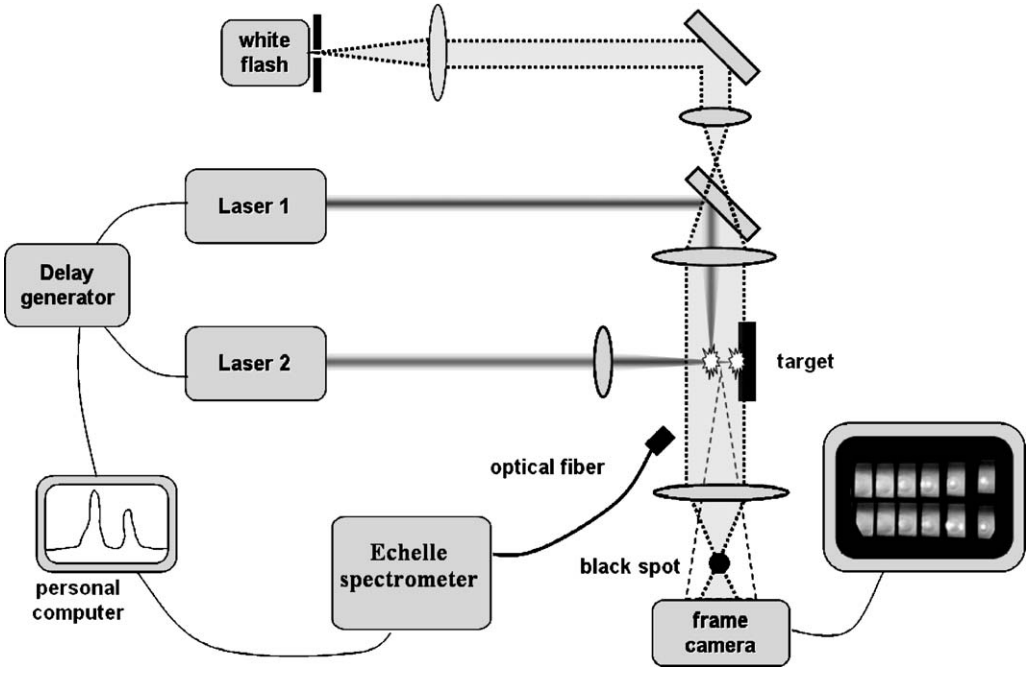

Fig. 1. Experimental setup.

For all measurements, performed at a repetition frequency of 2 Hz, 45 spectra were averaged, in order to reduce the fluctuations of the signal. The target was moved after each measurement to a "fresh" surface point. In this way, the intensity fluctuations of the spectroscopic signal were 10% or lower.

For the acquisition of shadowgraphic images, a white light from a photographic flash was used for back-illuminating the plasma during its evolution. The plasma images were then acquired using a Hadland Photonics frame camera adapted for fast imaging of the plasma and recorded on Polaroid high-sensitivity plates. This apparatus allowed the simultaneous time resolved imaging of the bright plasma plume and of the shock wave (SW) expanding front. The shadowgraphy apparatus was setup in the Schlieren scheme (a black spot stops the direct light on the frame camera); the shock wave is thus visible as a bright spherical or hemispherical layer on a dark background.

3. Results

As said before, for a better understanding of the physical mechanisms underlying the improvement of plasma emission in the DP orthogonal pre-ablation configuration, LIBS spectra and shadowgrams were obtained by varying both the distance d of the pre-ablation beam with respect to the target and the interpulse delay Δt. It is expected, in fact, that these two parameters would affect strongly the dynamic evolution of the plasma and the shock wave induced by the ablation laser and, consequently, the emission enhancement obtained.

3.1. Analysis of signal enhancement

Different lines originating from atomic and ionized species of both copper and zinc were analyzed. Zn I @ 472.2 nm and Zn II @ 255.8 nm were chosen as representative of neutral and ionized lines, respectively. The energies of the lower level of both the transitions are relatively high (32,501 and 49,355 cm^{-1}, respectively) so that the self-absorption effect can be neglected even if Zn is one of the major elements of the matrix.

No appreciable difference was observed between the signals obtained with the two laser fired simultaneously or using only the laser perpendicular to the target surface; thus, in the following, the second laser beam has been taken as reference to calculate the signal enhancement DP/SP (i.e. the ratio between the line intensity obtained in the DP configuration and that obtained using only the ablation laser).

The DP/SP ratio of both Zn lines is shown in Figs. 2 and 3 as a function of the interpulse delay (up to 50 μs) and for different distances d (up to 2.4 mm). No appreciable intensity enhancement has been found for values of the distance d larger than 2.4 mm. The x-axis in the figures is in logarithmic scale to better appreciate the intensity ratio at short interpulse delays.

A significant signal enhancement for the two lines is observed for distances d lower than 1 mm reaching a maximum DP/SP-value of ~ 4.5 for the neutral line ~ 8.5 for the ionized line. It is evident that the distance d strongly affects the signal enhancement since a markedly low DP/SP value is observed if the waist of parallel laser beam is farther than 1–1.3 mm from the target surface. This behavior is highlighted by plotting the maximum enhancement vs. distance d, as shown in Fig. 4 for both Zn lines, where a sharp reduction occurs around the value $d = 1.0$ mm.

Other interesting information can be drawn from the behavior of the signal enhancement with the interpulse delay time. It is evident from Figs. 2 and 3 that the signal enhancement begins to increase already for a delay of 100 ns for $d = 0.1$ and 0.4 mm while for increasing distances the signal enhancement occurs at progressively higher interpulse delays.

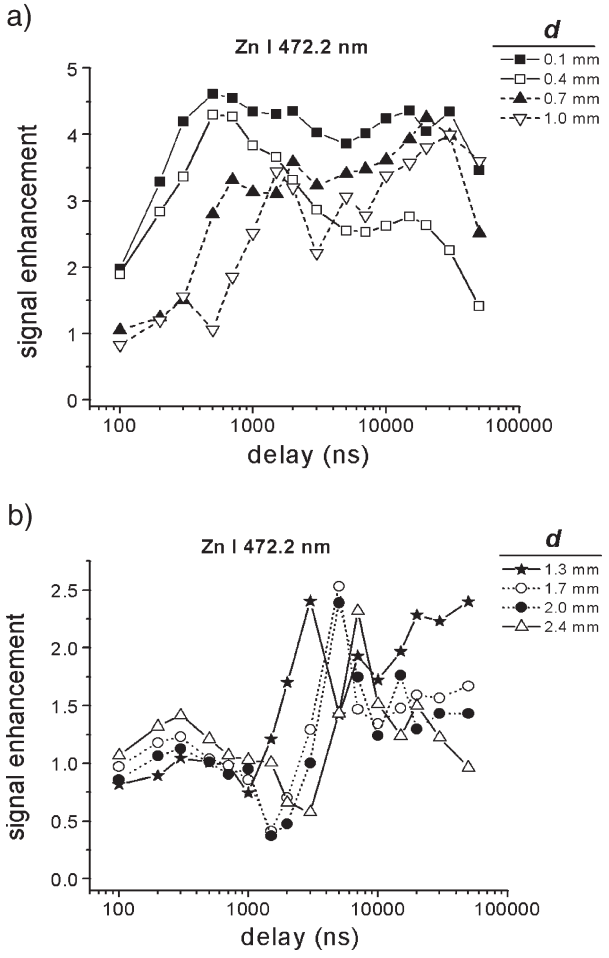

Fig. 2. Signal enhancement (DP/SP) of Zn I @ 472.2 nm vs. the delay between the laser pulses and at different values of the distance d.

Moreover, for the higher values of the distance d, a reduction of the signal is visible (DP/SP~0.35–0.6 for the atomic line and DP/SP~0.10–0.4 for the ionic line) at values of the interpulse delay Δt immediately before the onset of signal enhancement (see Figs. 2 and 3). Also the delay Δt associated to this signal dip seems to increase with the distance d. A similar signal reduction was previously found by Stratis et al. [9] who hypothesized a shielding of the sample from the ablation laser pulse by the air plasma.

In order to gain a better insight into the physical processes occurring in the orthogonal pre-ablation DP LIBS experiments and the reasons of the signal enhancement with respect to SP case, the different trend of the signal enhancement with the inter-pulse delay observed at different distances d values must be taken in consideration, together with the different dynamic evolution of both the plume and the shock waves.

In the hypothesis that the mechanism bringing to the signal enhancement is related to changes of buffer gas conditions driven by the air plume expansion rather than to the laser–target interaction (i.e. target pre-heating mechanism), the results obtained in the orthogonal DP case should approach those observed in the collinear DP case as the distance d approaches zero. In this view, it is encouraging to note that, similarly to what obtained in experiments in the collinear configuration [4,7], for d=0.1 mm the signal enhancement of the ionic line is higher than that of the neutral one and the optimal Δt value for the ionic line is higher than that found for the atomic line.

These aspects will be discussed in detail in the following sections.

3.2. Study of the thermodynamic parameters of the plasma

Both the spatially integrated temperature and electron density were calculated from the LIBS spectra acquired at different interpulse delays and different distances d.

The electron density was derived from the observed Stark broadening of the Cu I @ 427.5 nm line according to the approximated formula $W_{\mathrm{tot}} = w_{\mathrm{s}} \cdot \left(\frac{n_{\mathrm{e}}}{10^{16}}\right)$ where W_{tot} is the experimental line half-width and w_{s} is the Stark parameter tabulated by Konjevic and Wiese [23].

The results, shown in Fig. 5, should be compared with the value 4.2 10^{17} cm^{-3} obtained in the SP case. The relative errors of about 15% between the electron density values (not considering the systematic error on the Stark broadening parameter w_{s}) come from the reproducibility of the measurements, from the uncertainty in the determination of the line

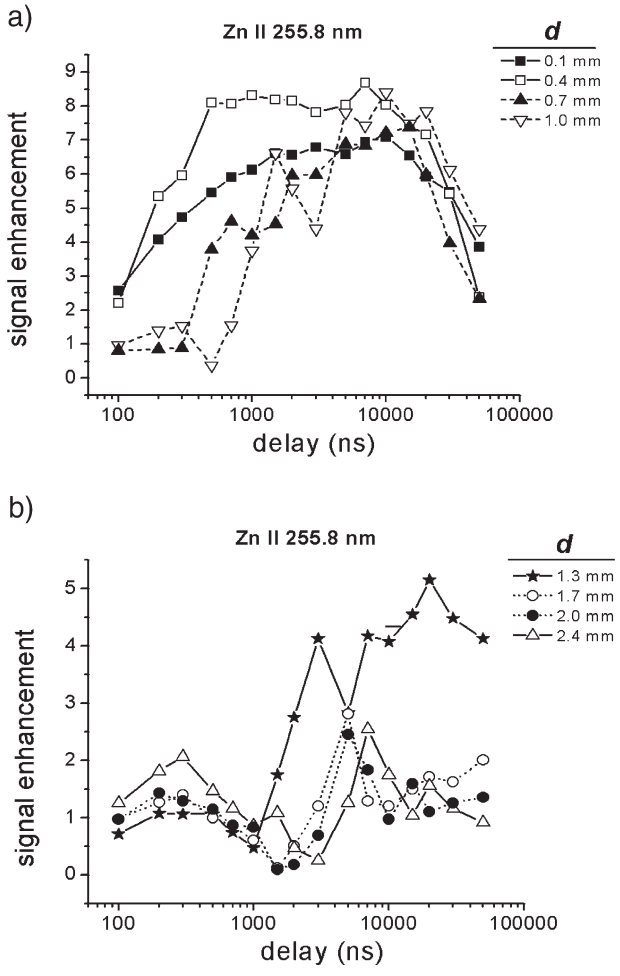

Fig. 3. Signal enhancement (DP/SP) of Zn II @ 255.8 nm vs. the delay between the laser pulses and at different values of the distance d.

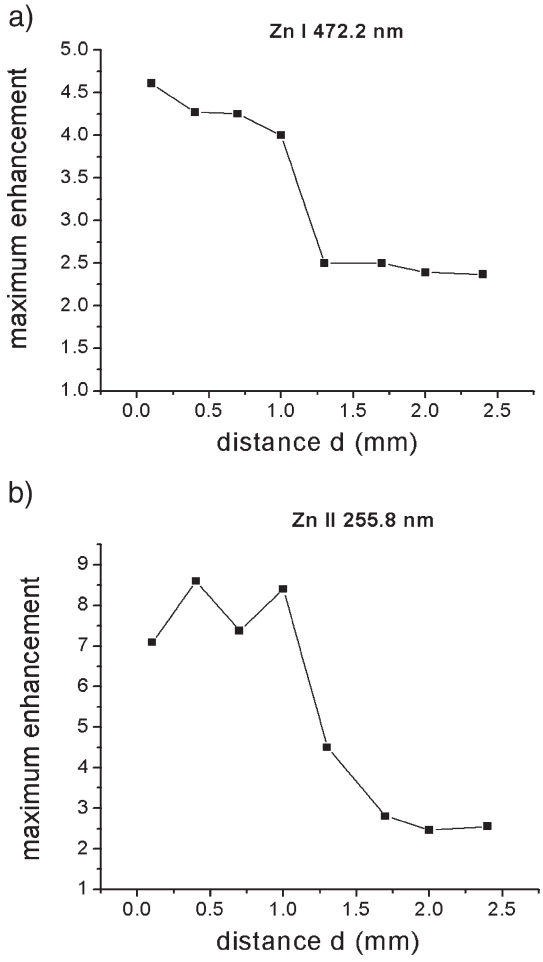

Fig. 4. Maximum signal enhancement of Zn I @ 472.2 nm and of Zn II @ 255.8 nm vs. the distance *d*.

broadening and from the dependence of the w_s parameter on the temperature.

While the trend of the electron density shows a monotonic decrease with the interpulse delay for distances *d* lower than 1 mm, a more complex behavior appears at longer distances where well discernible electron density dips are present at progressively longer delays (see Fig. 5).

The plasma temperature has been also calculated, in the framework of the Local Thermal Equilibrium (LTE) approximation, using the Saha–Boltzmann plot method, as described in Ref. [24]. This method consists in a generalization of the Boltzmann plot which takes into account both neutral and ionized lines, through the use of the Saha equation and using the values of plasma electron density previously calculated. The lines used for temperature calculation were Zn I @ 472.2 nm and Zn II @ 255.8. Using this technique, the difference between the upper level energies of the transitions considered is ~ 110.500 cm^{-1}, bringing to a considerable reduction of the fitting error with respect to the usual Boltzmann plot method. The experimental errors on temperature calculation (not considering the systematic error coming from the uncertainty of the A_{ki} coefficients) are of the order of 3%, coming mainly from the uncertainties of the electron density and the fitting of the line profile.

The calculated plasma temperatures are plotted in Fig. 6, as a function of the interpulse delay and for different values of the distance *d*. The results should be compared with the value of $T = 1.32$ eV obtained in the SP case. The temperature increase with respect to SP LIBS (~ 1.32 eV) is modest when present; on the other hand, an evident feature which can be observed in Fig. 6 is the presence of dips in the temperature at distances $d > 0.7$ mm as already observed (and at the same interpulse delays) for the emission enhancement (see Figs. 2 and 3) and for the electron density (see Fig. 5).

In order to understand the origin of the signal enhancements observed in Fig. 2, one can estimate the increment in the total number of emitting atoms (as an indication of the mass ablated), from the 472.2 nm Zn line intensity and the calculated values of temperature and electron density. In fact, it is possible to re-arrange the relation expressing the ratio of line intensity between DP and SP emission as follows:

$$\frac{N_{Zn}^{DP}}{N_{Zn}^{SP}} = \frac{I_{ki}^{DP}}{I_{ki}^{SP}} \frac{n^{SP}(T^{SP}, n_e^{SP})}{n^{DP}(T^{DP}, n_e^{DP})} \frac{Z(T_{DP})}{Z(T_{SP})} \exp\left(E_k\left(\frac{1}{k_B T_{DP}} - \frac{1}{k_B T_{SP}}\right)\right). \quad (1)$$

Here, N_{Zn} is the absolute total number of Zn atoms, *n* is the fraction of neutral atoms, I_{ki} is measured line intensity, *Z* is the

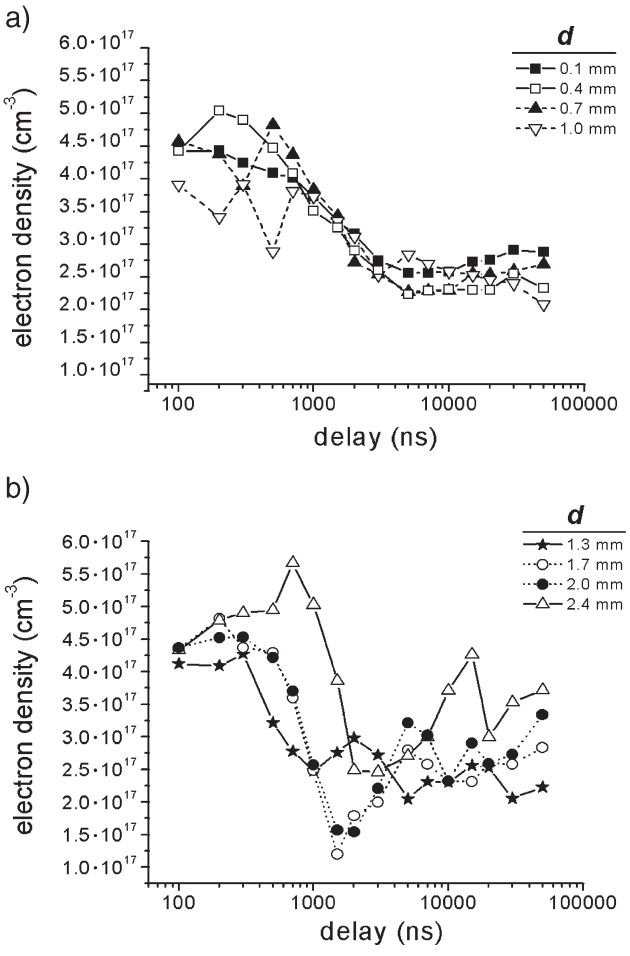

Fig. 5. Electron density as a function of interpulse delay at different distances *d*.

partition function, E_k is the upper energy level of the transition, k_B is the Boltzmann constant and finally the superscripts DP and SP indicate the double and single pulse case. In turn, the ratio n^{SP}/n^{DP} can be expressed in terms of temperature and electron density values via the Saha equation. The above expression assumes negligible effects due to plasma inhomogeneity and signal observation geometry. Moreover, it assumes that the stoichiometry of the ablation process is the same for SP and DP case. Needless to say, expression (1) can only provide an order of magnitude estimation of the enhancement, since the uncertainties are of the order of 30% even if the assumptions made are valid. Despite this, such calculation will provide an insight in the gross behavior of the mass ablated and its dependence on the thermodynamic parameters.

The ratio of mass ablated in DP over that in SP, obtained by means of expression (1) is reported in Fig. 7 for all the combinations of the interpulse delay and the distance d used.

A comparison of Fig. 7 with Figs. 2 and 3 shows clearly that the origin of the signal enhancement is mainly due to the higher ablated mass in the DP configuration, as already observed in the collinear DP experiments. Moreover, the higher enhancement of the ionic lines with respect to the atomic ones is due to the increase of the ionization ratio with respect to SP case,

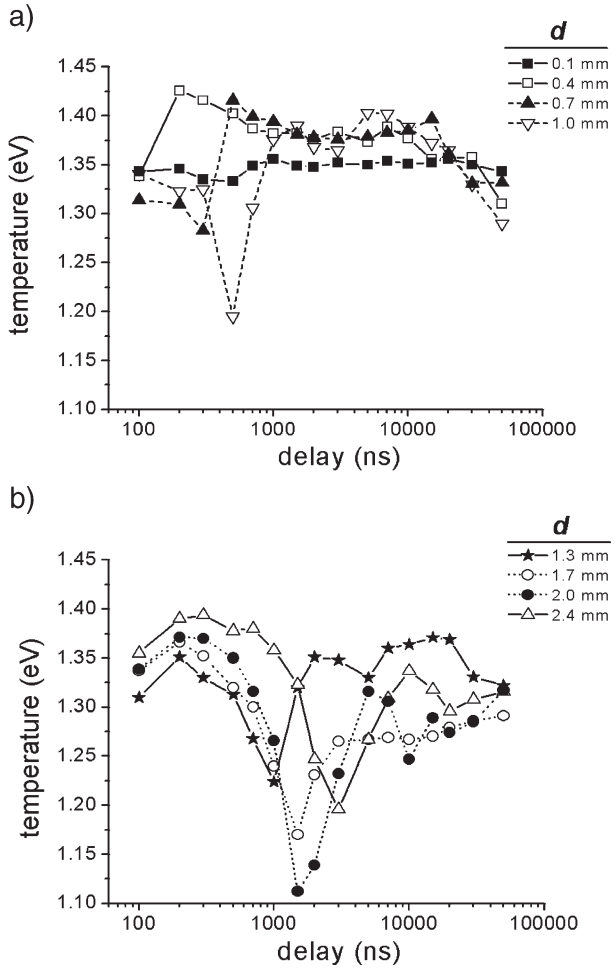

Fig. 6. Temperature vs. interpulse delay time for different values of the distance d.

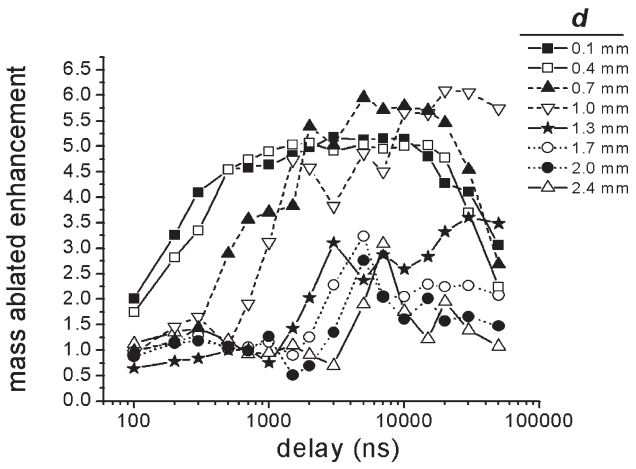

Fig. 7. Enhancement of ablated mass calculated from Eq. (1) as a function of interpulse delay and at different values of the distance d.

originated by the slight raise of temperature (Fig. 6) and the fall of electron density (Fig. 5). This is also evident observing that the atomic line emission enhancement is slightly lower than the ablated mass enhancement while the ionic line enhancement is markedly higher than that.

Another interesting feature observable from Fig. 7 is that the step reduction of signal enhancement for distances $d>1$ mm is due to a step reduction in the ablated mass and that the general behavior of the emission signal with the interpulse delay is the same of that of the ablated mass. A difference worth of noticing is the strong reduction or even the disappearance of the signal dip observed at the higher d values in Figs. 2 and 3; this means that such signal decrease is mainly (or solely) due to a reduction of the temperature (see Fig. 6) and not to a reduction of the ablated mass.

Such trend of the ablated mass, temperature, as well as electron density, will be discussed again later.

3.3. Analysis of shadowgraphic images

The shadowgraphic technique was used to monitor the evolution of the plasma obtained in orthogonal DP pre-ablation scheme under different experimental conditions, i.e. in a range of Δt between 1 and 8 μs and for distances d from 0.1 to 4.2 mm. In all cases, both the plume produced in air by the first laser pulse and the plume produced near the target by the second laser pulse are clearly visible, as well as the two shock waves departing from their positions.

In the following a cylindrical coordinate system will be used for describing the SWs and plumes expansion were the Z direction coincides with the axis perpendicular to the target surface and the radial expansion indicates the expansion in all the directions parallel to the surface plane.

The evolution observed in the images is strongly dictated by the choice of the distance d. The different situations observed can be grouped in four cases, represented in Fig. 8 a–d.

In case a) the ablation laser is fired before the arrival of the shock wave SW1 created with the air spark on the target. The expansion of the plume and the shock wave SW2 produced by

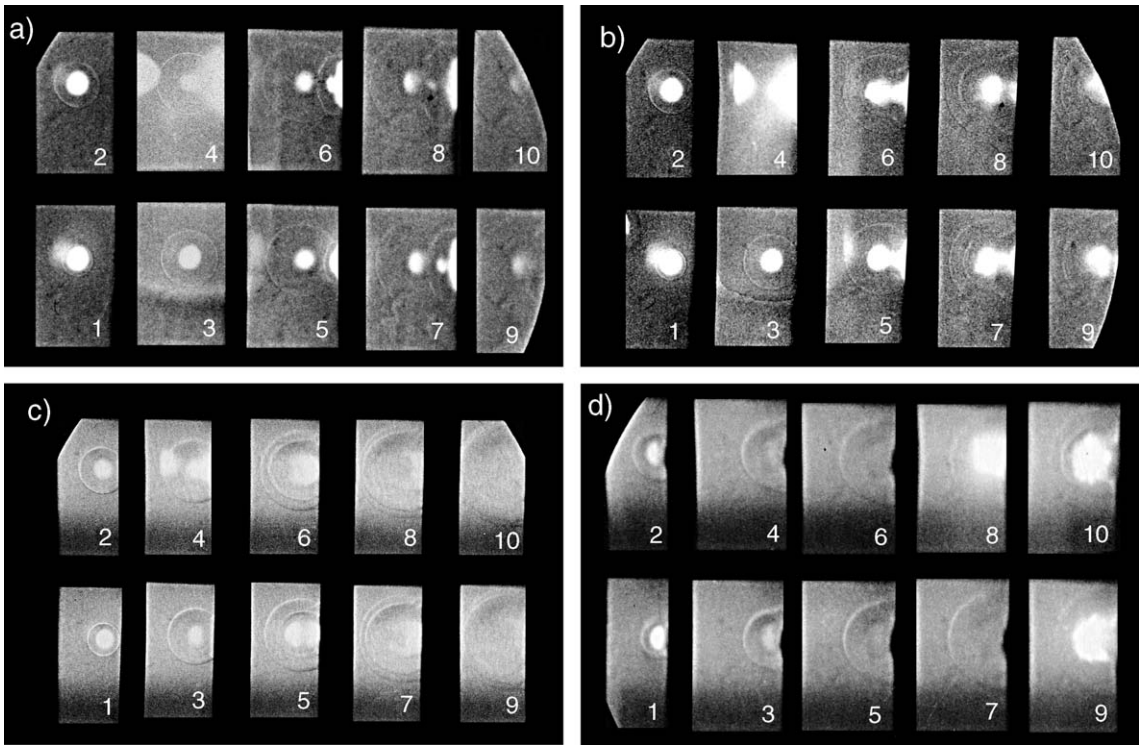

Fig. 8. Shadowgraphic images showing the evolution of the plume and of the first and second shock waves produced with an interpulse delay of 2 μs and a distance *d* of 4.2 mm (a), 2.8 mm (b) 1.9 mm (c), and with an interpulse delay of 4 μs and a distance *d* of 0.7 mm (d). The temporal delay between the frames is 500 ns.

the ablation pulse slows down as a result of SW1, which is propagating toward the target surface. The SW1 front in fact, as predicted by the theory of strong point explosion, is characterized by a high gas density, traveling at supersonic velocity. SW2 slows down because it expands in a medium flowing in the opposite direction and, at early times, with a higher gas density (Sedov self-similar solution predicts that at fixed time the SW radius r and the ambient gas density ρ are related to each other by $r \propto \rho^{-1/5}$). It seems then reasonable that the expansion of both the second plume and the second shock wave is faster in the radial directions, where there is no density increase with respect to atmospheric conditions, than in the Z direction. The result is that the target plume and SW2 expand assuming a flat shape similar to a disc; moreover in this case the target plume cannot coalesce with the air plume, which is then not re-heated.

In case b), the second laser is fired just after the arrival on the target surface of the shock wave SW1. As in the previous case, the second plume has initially a flat shape, again probably due to a slowdown, but soon it coalesces with the plume produced by the first pulse, reheating it (compare the brightness of air plume in frames 5,6,7,8 of Fig. 8b with those in Fig. 8a). The expansion of the SW2 is different in the radial and Z directions, but contrarily to case a), SW2 now finds soon in the Z direction the rarefied slow moving region located in the middle of the air spark and accelerates its motion, assuming an elongated shape.

In case c), the ablation laser is fired well after the time taken by SW1 to reach the target. Here, the situation is similar to case b) but the elongation is much less evident since the rarefied region of the first plume is nearer to the target. The two plumes rapidly coalesce and the two shock waves become almost concentric.

Finally, in case d) the ablation laser is fired well after both SW1 and the air plasma have reached the target. In that case, the evolution is similar to case c) but the final plume is larger and brighter even for higher values of the interpulse delay (frame 8–10 in Fig. 8d).

A rough estimation of the maximum radius of the air spark from the shadowgraphic images (the bright region coincides with the *Bremsstrahlung* emission zone) gives a value ~ 1 mm. One can therefore conclude that the range of distances d, derived from spectroscopic analysis, for which a large signal enhancement is obtained coincides with the interaction condition described in case d). In other words the enhancement is considerable if the distance of the pre-ablation laser from the target surface is less than the value that the radius of the plume it creates assumes at the time of arrival of the second laser pulse.

4. Discussion

The results presented in the previous section have to be considered within the framework of the temporal and spatial evolution of the plasma created with a single laser pulse.

The shadowgraphic image reported in Fig. 9 shows the expansion of the plume and the shock wave induced in air by the parallel laser pulse and the following interaction of the shock wave with the target surface. As previously reported elsewhere [25], as time progresses, the shock wave, initially in contact with the plasma region (roughly indicated by the bright spot in Fig. 9, coinciding with the *Bremsstrahlung* emission

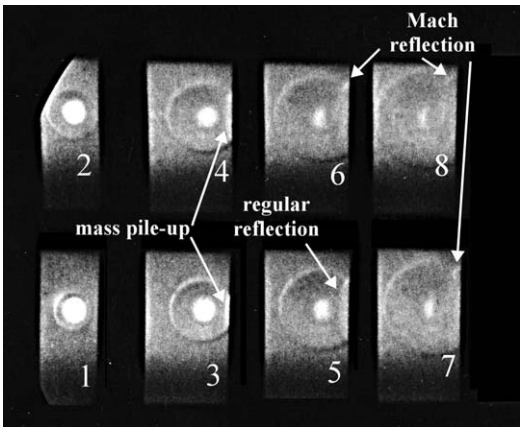

Fig. 9. Evolution of the plume and shock waves induced in air by a single laser pulse and their interaction with the target surface for a distance d=2.4 mm.

region), detaches from it and continues to expand, while the plume stops at a radius ~ 1 mm. This can be seen clearly in Fig. 10 where the radius of the plume and of the shock wave have been estimated from the images of Fig. 9.

The experimental values of the SW radius are in good agreement with the expansion law $r \propto t^{2/5}$ predicted by the Sedov strong point explosion theory, as seen from the fit of the data with a curve of the type $y=at^b$: the result, indicated in Fig. 10 by a dashed line, leads to a value of the exponent $b=0.4\pm0.02$. This is a confirmation of the adequacy of such theory in describing the process.

According to the Sedov's theory, after the explosion a large part of the mass which was previously contained in the region encompassed by the shock wave is piled-up at the shock front, as visible in Fig. 9 as a bright shell, while the shocked region is characterized by a high-temperature rarefied gas. Unfortunately, as discussed in a previous paper [26,27], the Sedov self-similar solution, while it can be used to describe the shock wave expansion and the profiles of temperature and gas density in the zone near the shock front, it is unable to give quantitative and

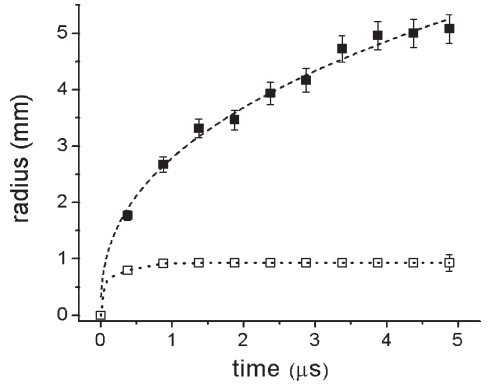

Fig. 10. Expansion of the pre-ablation shock wave (squares) and plume (empty squares), as estimated from Fig. 9. The dashed curve is the fit of shock wave position with a power function $y=at^b$. The dotted line represents a guideline for the eye showing the expansion of the plume. The relative errors on the SW radius are ~10% while the errors on the plume radius are ~15%.

reliable values of such parameters in the core of the plasma. In fact, the basic theory of strong point explosion neglects internal heat transfer phenomena such as conduction, radiation as well as excitation and ionization of the gas, and predicts an infinite temperature and a null density in the core of the plume. To correct this problem, more sophisticated models [28,29] accounting for the internal heat transport have been developed and predict a finite temperature. Moreover, considering the ideal gas state equation $\rho \propto P/T$, a non-zero gas density is also predicted in the core of the plume.

A qualitative sketch of the thermodynamic profiles in the spark region is reported in Fig. 11, where the steep increase of temperature at the plume border leads to an abrupt decrease of gas density in the core. Such density profile (accounting for both the air and plume atoms) is consistent with the predictions and results of the numerical model by Bogaerts and Chen [30], even if it considers only the first 100 ns after the laser ablation. When the shock wave reaches the target, the mass contained at the shock front starts to pile-up at the surface edge until a reflected wave which moves backward is formed. Numerical models [31,32] of blast wave reflection reveal that such an initial accumulation of mass at the surface forms a layer characterized by pressure and density higher than the original shock front. This situation can be confirmed by the presence of a bright layer near the target (indicating a high density in shadowgraphy experiments) in frames 3 and 4 of Fig. 9, while the regular reflected wave is evident in frames 5 and 6. At the time of frame 5, the pressure and density at the contact layer start to decrease until a rarefaction is produced when the reflected wave detaches from the surface. It is also interesting to

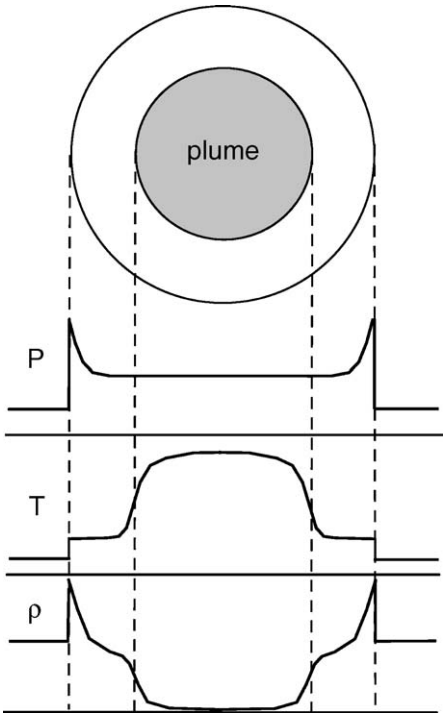

Fig. 11. Qualitative sketch of the profiles of pressure, temperature and gas density along the pre-ablation plume and shock wave.

note in frames 7 and 8 the presence of the non-regular reflected wave, known as Mach wave [31–33], which is formed at later times when the angle of incidence of the shock wave on the target becomes higher than a critical value ϕ_{cr}, which depends on the Mach number M (for $M>1.5$, $40°<\phi_{cr}<45°$).

The above considerations can now be applied to the results reported in Figs. 2 and 3. Experimentally, the enhancement is found to be higher when the ablation occurs close to the centre of the first spark reaching a high value when the ablation occurs physically in the core of the first plume ($d<1$ mm). Keeping in mind that the core of the plume is characterized by a gas density much lower than the unperturbed state and that the abrupt density decrease occurs at the plume edge (because of the abrupt increase of temperature), it appears that also in pre-ablation DP LIBS the signal enhancement can be related to the change in the buffer gas density where the ablation occurs. This outcome was already observed in previous works [15,16] devoted to the study of the double pulse technique in the collinear configuration, thus suggesting that the physical mechanism can be the same in the two cases.

In the collinear configuration, the observed signal enhancement was attributed to the rarefaction present behind the shock wave produced by the first laser spark [16].

It is known that, in single pulse LIBS, the emission is maximum when the buffer gas density assumes an optimum value which is lower than the atmospheric one, as found experimentally by Sdorra and Niemax [34] and by Iida [35]. In their interpretation, the key mechanism that must be considered is the laser shielding by the plasma which is strongly affected by the buffer gas, since a high buffer gas density favors the breakdown-cascade process, the formation of free electrons in the plasma and the absorption of laser radiation [35]. Therefore, reducing the density of the buffer gas, the laser shielding becomes less efficient and the mass removed from the target increases. On the other hand, if the buffer gas is too rarefied, the temperature of the induced plasma is too low, resulting into a lower emission. The optimal balance between these two effect is reached at a density value, depending on laser parameters and sample matrix, which is of the order of 10% of the atmospheric value [16] (corresponding at ambient temperature to a pressure around 100 hPa).

Such hypothesis for explaining the emission enhancement in the collinear DP LIBS is consistent with the growth of crater dimensions and ablated mass [8,18] and with the large dimensions of the laser induced plumes observed [5,15,17].

In the pre-ablation DP LIBS scheme the situation is similar: the arrival of the shock wave on the target initially leads to a density growth at the surface–gas boundary, but successively the wave reflection leads to a modest gas rarefaction. However, if the hot plasma region produced by the pre-ablation pulse is able to reach the target surface ($d<1$ mm), the rarefaction produced at the surface boundary becomes much stronger. In that case, the ablation process by the second pulse is very efficient and the rapid expansion of the new resulting plume in a rarefied medium leads to a large and dense plasma region. This is the reason for which, in Fig. 8d, the second plume is much brighter and larger than in cases a,b,c.

The gas rarefaction in the core of the plume can be evaluated from the ideal gas relation:

$$\frac{n_{\text{plume}}}{n_{\text{atmospheric}}} = \frac{P_{\text{plume}}}{P_{\text{atmospheric}}}\frac{T_{\text{atmospheric}}}{T_{\text{plume}}} \tag{2}$$

According to the strong explosion theory [20] (see Fig. 11), the pressure reaches a maximum P_{SW} at the SW front and then rapidly decreases behind it toward a value $P_{\text{plume}} \approx 0.365\ P_{SW}$ (this value is substantially independent on the blast wave energy down to a SW velocity around Mach 1.5). The corrections to the Sedov model accounting for the internal heat transfer processes do not bring large variations in pressure profiles [28,29], showing at most a slight decrease of the value of P_{plume}; this can be also perceived from the good agreement of the measured shock wave radius with the predicted one, since the driving force of the shock is essentially the pressure behind it.

Moreover, the SW front pressure P_{SW} and the unperturbed pressure $P_{\text{atmospheric}}$ are linked by the relation

$$P_{SW} = \frac{P_{\text{atmospheric}}(2\gamma M^2 - \gamma + 1)}{\gamma + 1} \tag{3}$$

where M is the SW Mach number and $\gamma=1.4$ is the adiabatic coefficient of air [20]. Calculating the Mach number by fitting the shock radius derived from Fig. 9, we obtain $M\sim 2.2$ and then $P_{SW}\sim 5.5 P_{\text{atmospheric}}$.

Finally, substituting this value in Eq. (2) and considering $T_{\text{atmospheric}}=300$ K and $T_{\text{plume}}\sim 15{,}000$ K (a reasonable value of the pre-ablation spark temperature) we obtain $\frac{n_{\text{plume}}}{n_{\text{atmospheric}}} = 0.04$, which is in good agreement with the optimal range found previously [16,34].

Looking at the dependence of the lines intensity on the distance d it is also clear that the rarefaction induced just by the arrival of the shock wave (and not by the presence of the air plume) is lower and then produces a lower signal enhancement; in this case the enhancement is caused by the slight rarefaction produced in front of the target, behind the reflected shock wave.

The process of SW reflection on a rigid wall discussed above together with the inspection of dynamic evolution of the plumes observable in Fig. 8a–d allow also to interpret the trend of the signal enhancement, of temperature and of electron density with the interpulse delay.

In the case of the largest distance in Figs. 2–3 (d=2.4 mm), four different phases can be identified. If the ablation laser is fired before the arrival of SW1 at the target surface (phase 1), the situation is similar to that shown in Fig. 8a: the mass ablated is the same as that in the SP case because the ambient conditions upon the target surface have not yet changed. Nevertheless, the plasma temperature and electron density are slightly higher than in the SP case since the plasma slows down due to the presence of SW1. As a result, a very small signal enhancement is observed. Otherwise, if the ablation laser is fired immediately after SW1 has reached the target surface but before a reflected wave is clearly visible and detached from the surface (phase 2)($\sim 1\ \mu s < \Delta t < \sim 3\ \mu s$ according to Figs. 9–10), the situation is similar to that shown in Fig. 8b and the ablation occurs in a high density environment. Higher

laser shielding and lower mass removal can then occur (see Fig. 7), although more accurate measurements are needed to confirm this aspect. However, as suggested by Fig. 8b, the induced plume overcomes the high density region and expands rapidly in the rarefied region corresponding to the air plasma. Such fast expansion causes the decrease of temperature, electron density and line intensity, as observed in Figs. 4, 5b and 6b. At still longer interpulse delays (phase 3) ($\Delta t > \sim 3$ μs), the signal starts to increase again reaching levels higher than the SP signal; this increase is associated with a stronger mass ablation, as visible in Fig. 7. Following our interpretation it is possible that at such interpulse delays the reflected wave is well formed and that a rarefaction region is formed in front of the target causing a more effective ablation. Moreover, the induced plume does not overcome the SW1 high density wall but is confined from it, so that the temperature and the electron density do not decrease and in some cases may even increase. If the interpulse delay is still increased (phase 4) the rarefaction progressively disappears, due to the refilling with gas of the contact region which then reverts to the unperturbed state, and the signal approaches the SP value (DP/SP = 1).

All the 4 phases described above occur at shorter interpulse delays with decreasing the distance d since the shock wave reaches more rapidly the target. While phase 1 rapidly disappears and phase 2 is evident for $d \geq 1$ mm, the increase in signal and ablated mass becomes much more evident with decreasing the distance because of the progressively stronger rarefaction present in front of the target.

It is interesting to note that the results obtained are consistent with the typical results of collinear DP experiments when d approaches zero, in which case phase 3 occurs immediately. In fact, in the case $d = 0.1$ mm, the behavior of the atomic and ionic lines, of the electron density and temperature is very similar to that observed in DP collinear LIBS.

5. Conclusions

In order to gain some physical understanding of the signal enhancement obtained in the DP pre-ablation LIBS, spectroscopic and shadowgraphic experiments were carried out by focusing a 140 mJ Nd:YAG laser in air at a distance d from the target and then a 240 mJ Nd:YAG laser on the sample surface. The distance d was varied in the range 0.1–4.2 mm and the delay between the two pulses was varied from 0 to 50 μs.

For all the combinations of such experimental parameters, the signal enhancement of Zn neutral and ionic lines was measured, the spatially averaged temperature and electron density were calculated, and the increase of the number of Zn atoms in the plume was estimated.

The estimated ablated mass and the dynamic evolution of the plume differ considerably by changing the distance and the interpulse delay time, leading to different levels of enhancement of line intensities. While a strong signal increase, attributed mainly to an increase of the ablated mass, was observed for distances d lower than approximately 1 mm, a marginal signal improvement was observed at longer distances of the pre-ablation spark from the target. Since the dimensions of the air plume are of the order of 1 mm, it is evident that the enhancement is strong whenever the target ablation occurs within the pre-ablation plasma environment.

An interpretation of the signal enhancement based on the changes in ambient gas density where the target ablation occurs was proposed, in agreement with previous results obtained in the collinear DP LIBS.

The different dynamic evolution observed allowed also to interpret the trend of the signal enhancement versus interpulse delay.

References

[1] J.D. Winefordner, I.B. Gornushkin, T. Correl, E. Gibb, B.W. Smith, N. Omenetto, Comparing several atomic spectroscopic methods to the super stars: special emphasis on Laser Induced Breakdown Spectroscopy, LIBS, a future super star, J. Anal. At. Spectrom. 19 (2004) 1061–1083.

[2] S. Nakamura, Y. Ito, K. Sone, H. Hiraga, K. Kaneko, Determination of an iron suspension in water by laser-induced breakdown spectroscopy with two sequential laser pulses, Anal. Chem. 68 (1996) 2981–2986.

[3] L. St-Onge, M. Sabsabi, P. Cielo, Analysis of solids using laser induced plasma spectroscopy in double-pulse mode, Spectrochim. Acta Part B 53 (1998) 407–415.

[4] L. St-Onge, V. Detalle, M. Sabsabi, Enhanced laser-induced breakdown spectroscopy using the combination of fourth-harmonic and fundamental Nd:YAG laser pulses, Spectrochim. Acta Part B 57 (2002) 121–135.

[5] R. Noll, R. Sattmann, V. Sturm, S. Winkelmann, Space- and time-resolved dynamics of plasmas generated by laser double pulses interacting with metallic samples, J. Anal. At. Spectrom. 19 (2004) 419–428.

[6] F. Colao, V. Lazic, R. Fantoni, S. Pershin, A comparison of single and double pulse laser-induced breakdown spectroscopy of aluminum samples, Spectrochim. Acta Part B 57 (2002) 1167–1179.

[7] C. Gautier, P. Fichet, D. Menut, J.L. Lacour, D. L'Hermite, J. Dubessy, Main parameters influencing the double pulse laser-induced breakdown spectroscopy in the collinear beam geometry, Spectrochim. Acta B 60 (2005) 792–804.

[8] R. Sattmann, V. Sturm, R. Noll, Laser-induced breakdown spectroscopy of steel samples using multiple Q-witch Nd:YAG laser pulses, J. Phys., D. Appl. Phys. 28 (1995) 2181–2187.

[9] D.N. Stratis, K.L. Eland, S.M. Angel, Dual-pulse LIBS using a preablation spark for enhanced ablation and emission, Appl. Spectrosc. 54 (2000) 1270–1274.

[10] D.N. Stratis, K.L. Eland, S.M. Angel, Effect of pulse delay time on a pre-ablation dual-pulse LIBS plasma, Appl. Spectrosc. 55 (2001) 1297–1303.

[11] D.N. Stratis, K.L. Eland, S.M. Angel, Enhancement of aluminum, titanium, and iron in glass using pre-ablation spark dual-pulse LIBS, Appl. Spectrosc. 54 (2000) 1719–1726.

[12] C. Gautier, P. Fichet, D. Menut, J.L. Lacour, D. L'Hermite, J. Dubessy, Quantification of the intensity enhancements for the double-pulse laser-induced breakdown spectroscopy in the orthogonal beam geometry, Spectrochim. Acta Part B 60 (2005) 265–276.

[13] H. Lindner, J. Koch, K. Niemax, Production of ultrafine particles by nanosecond laser sampling using orthogonal prepulse laser breakdown, Anal. Chem. 77 (2005) 7528–7533.

[14] C. Gautier, P. Fichet, D. Menut, J.L. Lacour, D. L'Hermite, J. Dubessy, Study of the double-pulse setup with an orthogonal beam geometry for laser-induced breakdown spectroscopy, Spectrochim. Acta Part B 59 (2004) 975–986.

[15] M. Corsi, G. Cristoforetti, M. Hidalgo, S. Legnaioli, V. Palleschi, A. Salvetti, E. Tognoni, C. Vallebona, A 3D-analysis of laser induced plasmas in single and double pulse configuration, Spectrochim. Acta Part B 59 (2004) 723–735.

[16] G. Cristoforetti, S. Legnaioli, V. Palleschi, A. Salvetti, E. Tognoni, Influence of ambient gas pressure on Laser Induced Breakdown

Spectroscopy technique in the parallel double pulse configuration, Spectrochim. Acta Part B 59 (2004) 1907–1917.
[17] G. Cristoforetti, S. Legnaioli, V. Palleschi, A. Salvetti, E. Tognoni, Characterization of a collinear double pulse laser-induced plasma at several ambient gas pressures, Appl. Phys., B Lasers Opt. 80 (2005) 559–568.
[18] P.A. Benedetti, G. Cristoforetti, S. Legnaioli, V. Palleschi, L. Pardini, A. Salvetti, E. Tognoni, Effect of laser pulse energies in Laser Induced Breakdown Spectroscopy in double-pulse configuration, Spectrochim. Acta Part B 60 (2005) 1392–1401.
[19] S.M. Pershin, Physical mechanism of suppression of the emission of radiation by atmospheric gases in a plasma formed as a result of two-pulse irradiation of the surface, Sov. J. Quantum Electron. 19 (1989) 1618–1619.
[20] L.I. Sedov, Similarity and Dimensional Methods in Mechanics, CRC Press, LCC, Moscow, 1993.
[21] J. Scaffidi, S.M. Angel, D.A. Cremers, Emission enhancement mechanisms in dual-pulse LIBS, Anal. Chem. 1 (2006) 25–32.
[22] A. Ciucci, V. Palleschi, S. Rastelli, A. Salvetti, D.P. Singh, E. Tognoni, Effect of imperfect focusing in laser-induced plasma spectroscopy measurements, Il Nuovo Cim., D 20 (1998) 1469–1478.
[23] N. Konjevic, W.L. Wiese, Experimental Stark widths and shifts for spectral lines of neutral and ionized atoms (a critical review of selected data for the period 1983 through 1988), J. Phys. Chem. Ref. Data 19 (1990) 1307–1385.
[24] S. Yalcin, D.R. Crosley, G.P. Smith, G.W. Faris, Influence of ambient conditions on the laser air spark, Appl. Phys., B 68 (1999) 121–130.
[25] M. Corsi, G. Cristoforetti, M. Hidalgo, D. Iriarte, S. Legnaioli, V. Palleschi, A. Salvetti, E. Tognoni, Temporal and spatial evolution of a laser induced plasma from a steel target on LIBS quantitative analysis, Appl. Spectrosc. 57 (2003) 715–721.
[26] S.B. Wen, X. Mao, R.E. Russo, Comment on "three-dimensional analysis of laser induced plasmas in single and double pulse configuration", 60 (2005) 870–872.
[27] M. Corsi, G. Cristoforetti, M. Hidalgo, S. Legnaioli, V. Palleschi, A. Salvetti, E. Tognoni, C. Vallebona, Author's reply to Wen et al.'s comment, Spectrochim. Acta Part B 60 (2005) 872–875.
[28] A.M. Abdel-Raouf, W. Gretler, Quasi-similar solutions for blast waves with internal heat transfer effects, Fluid Dyn. Res. 8 (1991) 273–285.
[29] A.F. Ghoniem, M.M. Kamel, S.A. Berger, A.K. Oppenheim, Effects of internal heat transfer on the structure of self similar blast waves, J. Fluid Mech. 117 (1982) 473–491.
[30] A. Bogaerts, Z. Chen, Effect of laser parameters on laser ablation and laser-induced plasma formation: a numerical modeling investigation, Spectrochim. Acta Part B 60 (2005) 1280–1307.
[31] V.V. Podlubnyi, A.S. Fonarev, Reflection of a spherical blast wave from a planar surface, Fluid Dyn. 9 (1974) 921–926.
[32] Z. Jiang, K. Takayama, K.P.B. Moosab, O. Onodera, M. Sun, Numerical and experimental study of a micro-blast wave generated by pulsed-laser beam focusing, Shock Waves 8 (1998) 337–349.
[33] M. De Rosa, F. Famà, V. Palleschi, D.P. Singh, M. Vaselli, Derivation of the critical angle for Mach reflection for strong shock waves, Phys. Rev., A 45 (1992) 6130–6132.
[34] W. Sdorra, K. Niemax, Basic investigations for laser microanalysis. III. Applications of different buffer gases for laser-produced sample plumes, Mikrochim. Acta 107 (1992) 319–327.
[35] Y. Iida, Effects of atmosphere on laser vaporization and excitation processes of solid samples, Spectrochim. Acta Part B 45 (1990) 1353–1367.